Energy 102 (2016) 166–175

Contents lists available at ScienceDirect

Energy

journal homepage: www.elsevier.com/locate/energy

The influence of blade pitch angle on the performance of a model horizontal axis tidal stream turbine operating under wave–current interaction

Tiago A. de Jesus Henriques [a], Terry S. Hedges [a], Ieuan Owen [b], Robert J. Poole [a, *]

[a] School of Engineering, University of Liverpool, Brownlow Hill, L69 3GH, United Kingdom
[b] School of Engineering, University of Lincoln, Brayford Pool, LN6 7TS, United Kingdom

ARTICLE INFO

Article history:
Received 11 June 2015
Received in revised form
18 January 2016
Accepted 10 February 2016
Available online xxx

Keywords:
Tidal energy
HATT (Horizontal axis tidal turbine)
ADV (Acoustic Doppler velocimeter)
Wave-current interaction
Stokes' wave theory

ABSTRACT

Tidal stream turbines offer a promising means of producing renewable energy at foreseeable times and of predictable quantity. However, the turbines may have to operate under wave-current conditions that cause high velocity fluctuations in the flow, leading to unsteady power output and structural loading and, potentially, to premature structural failure. Consequently, it is important to understand the effects that wave-induced velocities may have on tidal devices and how their design could be optimised to reduce the additional unsteady loading.

This paper describes an experimental investigation into the performance of a scale-model three-bladed HATT (horizontal axis tidal stream turbine) operating under different wave-current combinations and it shows how changes in the blade pitch angle can reduce wave loading. Tests were carried out in the recirculating water channel at the University of Liverpool, with a paddle wavemaker installed upstream of the working section to induce surface waves travelling in the same direction as the current. Three wave conditions were employed in a current-dominated flow. The wave kinematics were measured using an acoustic Doppler velocimeter and there was generally good agreement with Stokes' second-order wave theory. Power and thrust measurements were taken under both current-alone and wave-current conditions for different blade pitch angles. It was observed that, as the blade pitch angle was increased from optimum, both the mean power and thrust on the turbine decreased and the reductions in thrust were always greater than in power. The fluctuations in power and thrust also decreased with an increase in the blade pitch angle. Therefore, changes in blade pitch angle can be used as a mechanism for reducing the loading on a HATT when operating with excessive wave-induced loads, while still enabling a significant amount of the available power in the unsteady tidal stream to be extracted.

1. Introduction

Increasing demand for energy has led to considerable interest in renewable energy sources. Tides are predictable, unlike many other sources of renewable energy, and tidal turbines offer a promising means of converting the tidal stream kinetic energy into electrical energy. In April 2008, Marine Current Turbines Ltd installed the first tidal stream turbine which successfully provided power extracted from tidal currents to the UK national grid. In 2012, OpenHydro installed a tidal farm at Paimpol-Bréhat (France) which generates 43 GWh annually. Further sites have tidal stream devices installed and more potential sites are being investigated [1].

Several laboratory-scale experiments have evaluated the power and thrust performances of tidal stream devices and their near-wake characteristics under uniform flow velocities [2–5]. However, the seas around the UK, and other potential sites around the world, are exposed to considerable wave activity, and currents can be significantly influenced by the presence of waves. Waves induce orbital motions within the water column and thus introduce both horizontal and vertical components to the flow [6–8]. The precise nature of the orbital motion depends on the characteristics of the waves and the site. Thus, understanding the effects of the wave-induced velocities on the performance of tidal stream

* Corresponding author.
E-mail addresses: pp0u8184@liv.ac.uk (T.A. de Jesus Henriques), ec22@liv.ac.uk (T.S. Hedges), iowen@lincoln.ac.uk (I. Owen), robpoole@liv.ac.uk (R.J. Poole).

http://dx.doi.org/10.1016/j.energy.2016.02.066

devices is essential for their design. Tidal turbines placed near the sea surface, where the current velocity is often greatest, would be particularly susceptible to wave-induced effects in the flow, producing fluctuations in both the power extracted and the loading on the turbine structure and hence increasing the potential for fatigue failure of structural elements.

In towing tank experiments [9–14], investigators have used three- and two-bladed horizontal axis tidal turbines (HATTs) with a range of scaled wave conditions to investigate the variations in turbine power output and thrust, as well as the bending moments on the individual blades. These studies showed how the time-averages of the unsteady power output and thrust were consistent with those measured with no waves, and how the fluctuating power and thrust amplitudes increase with wave amplitude. Research has also been conducted into simulated wave-current flows in a recirculating water channel by placing the turbine on a reciprocating motorised carriage [15]. The results showed that the inertia forces, due to the simulated wave-induced accelerations in the flow, were much lower than the additional fluctuating drag forces. In studies using recirculating water channels with waves created by a wavemaker, the kinematics of different wave-current conditions have been measured directly and it was observed that the main fluctuations in power and thrust occurred with frequencies that matched the frequencies of the waves [16–18].

Wind turbine technology is much more advanced than tidal turbine technology and, in that industry, the turbines can also experience fluctuating loads due to wind gusts and to the atmospheric boundary layer, leading to problems of unsteady structural loading and fatigue. As a result, methods of blade control have been developed to vary the pitch angle of the individual blades as the turbine rotates [19–21] and these techniques have been demonstrated to reduce the magnitude of the fluctuations. However, adjusting the blade pitch angle away from the optimum will affect not only the thrust imposed on the blade but also the power extracted. Thus, there is a trade-off between reduced fluctuating loads and power output.

The conditions under which tidal turbines operate are much harsher than those experienced by wind turbines, and sophisticated blade control strategies will be harder to implement. Nevertheless, blade pitch angle can be controlled and so, in this study, the blade pitch angle of a model-scale HATT has been incrementally adjusted while operating in different wave-current flows and the resultant effects on loading and power output have been measured. The model turbine uses a rotor control system with constant torque and variable speed, which reflects the design chosen by major tidal energy companies [22–24]. The turbine performance was first determined with its optimum blade pitch angle of 6° for the different flow conditions. The turbine's power output and thrust, both in terms of their means and standard deviations, were then measured for different blade pitch angles and compared with the optimal configuration.

Our aim in the present paper is to study experimentally the effect of varying the blade pitch angle from optimum conditions. In particular, we are interested in how varying this angle can be used to attenuate wave-induced unsteady loading whilst still extracting significant power. As it is well known that thrust scales with the free-stream velocity squared and power output with velocity cubed, one might expect that percentage reductions in power would always exceed those of thrust. Our results show that this does not have to be the case. Therefore, blade pitch control offers the potential of a step forward for the state-of-the-art in this area.

2. Wave theory

As noted earlier, surface waves induce orbital motions in the flow, introducing both horizontal and vertical velocity components (u_a and v_a) which decay through the water depth. The precise nature of the wave-induced orbital motion in the water column depends on the characteristics of the waves and the site. The ratio between the water depth (d) and wavelength (L) is one of the main parameters governing the behaviour of the wave-induced velocities. In deep water, $d/L > 0.5$, and in the absence of a current, both the horizontal and vertical velocity components decay exponentially through the water depth and there is very little motion beyond a depth equal to about half the wavelength. For waves in intermediate water depths, $0.04 \leq d/L \leq 0.5$, the water particle orbits in the absence of a current are essentially elliptical, with the vertical velocity decaying from a maximum at the water surface to zero at the sea bed, if the bed is impermeable. In shallow water, $d/L < 0.04$, the horizontal component of the wave-induced flow is essentially constant throughout the water depth whilst the vertical component again decays from a maximum at the water surface to zero at an impermeable bed [6–8].

A train of regular waves travelling in the same direction as a uniform steady current will have an apparent period (T_a) in a stationary frame of reference. The wave height (H) and apparent period, along with water depth (d) and the current velocity ($\overline{u}$), define the waveform. The wave profile is given by linear wave theory as follows [6–8]:

$$\eta = \frac{H}{2}\cos(kx - \omega_a t), \tag{1}$$

in which η is the water surface elevation above mean-water-level at any time (t), $k\,(=2\pi/L)$ is the wave number, L is the wavelength, x is the horizontal coordinate from the origin of the stationary coordinate system (positive in the direction of wave propagation), and $\omega_a\ (=2\pi/T_a)$ is the apparent wave angular frequency. The wavelength is calculated implicitly as follows [7]:

$$L = \left(\sqrt{\frac{g}{k}tanh(kd)} + \overline{u}\right) T_a, \tag{2}$$

where g is the acceleration due to gravity.

Linear wave theory is strictly appropriate only for waves of small amplitude. As waves become steeper ($H/L > 0.04$) then, provided that $HL^2/d^3 < 40$, regular waves are more accurately described by Stokes' higher-order wave theories [25]. According to Stokes' second-order theory, the water surface elevation for waves on arbitrary water depth is given by:

$$\eta = \frac{H}{2}\ cos(kx - \omega_a t) + \frac{kH^2}{16}\left[3\ coth^3(kd) - coth\ (kd)\right] cos2(kx - \omega_a t). \tag{3}$$

Although the wavelength given by Stokes' second-order theory can still be evaluated using equation (2), the higher-order effects cause changes in the wave kinematics from those predicted by linear theory. The resulting horizontal and vertical velocity components [6,8], added linearly to a uniform steady current, are:

$$u_a = \frac{H}{2}\omega_r \frac{cosh(ks)}{sinh(kd)} cos(kx - \omega_a t) + \frac{3H^2\omega_r k}{16}\frac{cosh(2ks)}{sinh^4(kd)} cos2(kx\text{-}\omega_a t) + \overline{u}, \tag{4}$$

$$v_a = \frac{H}{2}\omega_r \frac{\sinh(ks)}{\sinh(kd)} \sin(kx - \omega_a t) + \frac{3H^2 \omega_r k}{16} \frac{\sinh(2ks)}{\sinh^4(kd)} \sin 2(kx - \omega_a t), \quad (5)$$

in which s ($= d + y$) is the elevation above the bed, y is the vertical distance, positive upwards, measured from the mean-water-level and ω_r ($= \omega_a - k\overline{u}$) is the relative (or intrinsic) wave angular frequency [7]. Note that, the wave-induced orbital motions are no longer closed at second order even in the absence of a current: there is a mass transport in the direction of wave propagation.

3. Experimental set up

The experiments were performed in a recirculating water-channel at the University of Liverpool. A paddle wavemaker was installed at the upstream end of the channel working section to generate waves propagating in the same direction as the current. Flow velocity measurements were obtained using a Vectrino+ acoustic Doppler velocimeter (ADV). A model HATT with a diameter (D) of 0.5 m was subjected to both a uniform steady flow and to a current with superimposed waves and its performance was evaluated for different blade pitch angles via power and thrust measurements.

3.1. Recirculating water channel

The University of Liverpool's high-speed recirculating water channel, shown schematically in Fig. 1, has a capacity of 90,000 L and a working section 1.4 m wide, 0.76 m deep at the model location, and 3.7 m long. It is powered by a 75 kW electric motor driving an axial flow impeller and is capable of flow velocities up to 6 m/s with turbulence intensity of approximately 2%. The water flow at the inlet to the working section has a uniform velocity profile to within 1% except near the walls and floor where normal boundary layer effects occur [26]. The inlet velocity, $\overline{u}$, was set and maintained at 0.9 m/s; this corresponds to a Reynolds number, Re ($= \overline{u}R/\nu$ where ν is the kinematic viscosity and R is the turbine radius) of 2.3×10^5. Previous studies using the same experimental facilities have shown that the power and thrust results become fully Reynolds number independent at this velocity [27].

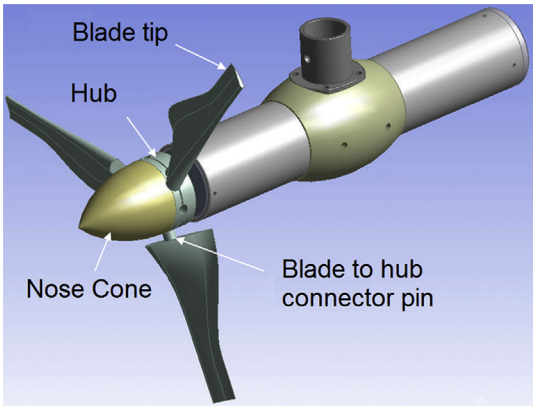

Fig. 2. Model HATT.

3.2. Scale model horizontal axis tidal turbine (HATT)

The turbine used during the experiments (shown in Fig. 2) has a horizontal axis and, for this study, was fitted with three blades. It has a diameter of 0.5 m and the optimum blade pitch angle for maximum power output in uniform flow is 6° [28]. The design of the turbine blade is a variant of the Wortmann FX 63–137 profile from the NACA (National Advisory Committee for Aeronautics) and has been studied in detail previously [29,30]. The turbine rotor is connected to a Baldor brushless AC servomotor which measures the rotor angular velocity (Ω) and uses a dynamic brake to apply a constant resistive torque. The angular velocity and torque were used to calculate the power output. A force block installed at the support stanchion measured the hydrodynamic loading on both the turbine structure and its support [27]. A 400 N strain gauge was used to measure the loading, which was calibrated against a series of known weights using an Instrunet system for data acquisition.

3.3. Wavemaker

The wavemaker, shown schematically in Fig. 3, consists of a hinged paddle which spans the water channel and lies on the water surface where the flow enters the working section. An electric motor rotates a crankshaft which moves the paddle up and down to produce regular surface waves. The frequency of the motor and the throw of the crankshaft can be adjusted to control the length and

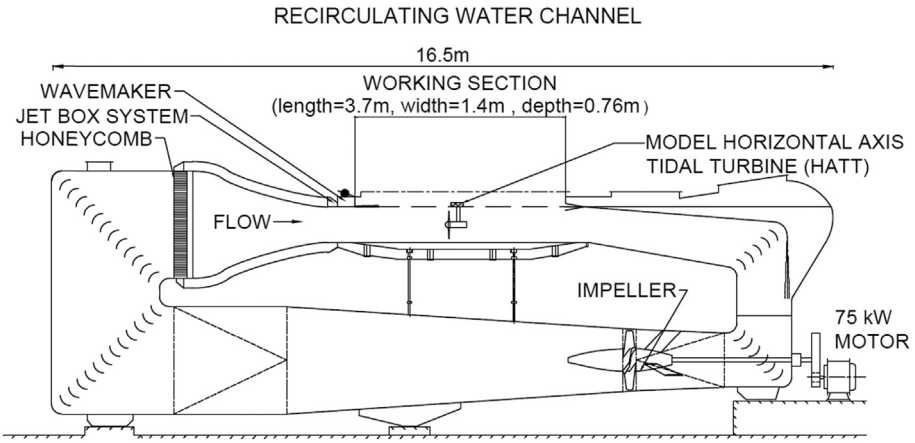

Fig. 1. Recirculating water channel schematic.

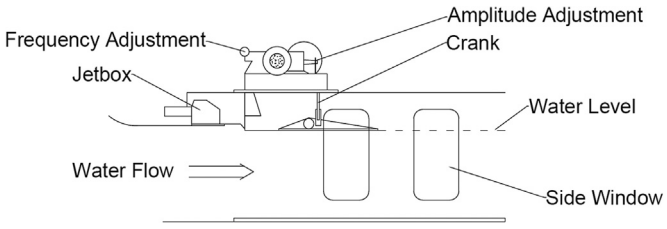

Fig. 3. Wavemaker schematic.

height of the waves. The changes in the water surface elevation were measured by a resistance probe calibrated with a range of ±5 V for the output signal. Data from the probe were collected at a sampling rate of 200 Hz using an Instrunet data acquisition system.

3.4. Acoustic Doppler velocimeter

Velocity measurements were obtained using a Nortek Vectrino+ acoustic Doppler velocimeter (ADV), which uses the acoustic Doppler principle to measure the water velocity in three dimensions. The ADV, shown in Fig. 4, has a titanium probe with four receiving transducers spaced at 90° intervals around a 10 MHz transmitter. The probe used in the tests had a downwards-looking orientation. Samples were collected at 200 Hz, with a sample volume of 0.2 cm^3 located 50 mm below the probe and with an estimated error of less than 1% in the mean velocity [31].

3.5. Methodology

The tests were performed with both a uniform current and wave-current interaction at $\overline{u} = 0.9$ m/s. To characterise the wave kinematics, measurements were first taken of the generated wave profiles 2 m downstream of the wavemaker paddle at several spanwise locations covering a 1 m width at the centre of the channel and without the turbine in place. The wave-induced water kinematics were measured at the same spanwise locations using the ADV and covered a depth range from $y = -120$ mm to −420 mm. Both ADV and wave probe data were collected for samples with a minimum of 250 waves (≈200 s). The data showed that the mean wave properties (height, apparent period and kinematics) had converged within ±0.5% after this number of waves.

The turbine was then installed at the same central location where the wave properties had been measured, with the rotor centre 400 mm deep. Turbine power and thrust were measured at a constant rotor torque setting, thereby causing the turbine to rotate with a varying angular speed. Measurements were taken at different blade pitch angles, both with the current alone and with three wave-current conditions. The three turbine blades were always set at the same blade pitch angle, which was varied between 3° and 18° in increments of 3°.

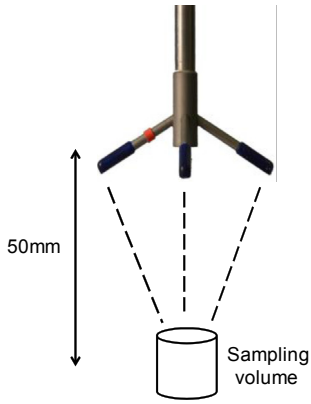

Fig. 4. ADV probe in downwards orientation.

Power output was measured at 100 Hz for sample sizes of 10,000 data points (i.e. ≈ 150 waves). Thrust measurements were taken at a sampling rate of 200 Hz for sample sizes of 30,000 points (i.e. ≈ 200 waves). The means of both the power and thrust statistically converged to within 1% after 50 wave cycles. The mean power and thrust coefficients ($\overline{C}_P$ and $\overline{C}_T$) were plotted against the mean tip speed ratio ($\overline{\lambda}$), calculated using the measured mean power ($\overline{P}$), mean thrust ($\overline{T}$), the mean rotor angular velocity ($\overline{\Omega}$), water density (ρ) and rotor swept area (A):

$$\overline{\lambda} = \frac{\overline{\Omega} R}{\overline{u}}, \tag{6}$$

$$\overline{C}_P = \frac{\overline{P}}{\frac{1}{2}\rho A \overline{u}^3}, \tag{7}$$

$$\overline{C}_T = \frac{\overline{T}}{\frac{1}{2}\rho A \overline{u}^2}. \tag{8}$$

In a similar manner, the standard deviations in the measured power and thrust were used to calculate the standard deviations of both coefficients (C'_P and C'_T) to quantify the fluctuations in power output and thrust.

Garret and Cummins [32] have shown that the effect of blockage is to increase the maximum potential power that the turbine can extract above the Betz limit for a turbine in an infinite flow field. Corrections for blockage, as given by Bahaj et al. [3], were initially applied to the data in the present study. However, these empirical corrections were found to be invalid for the non-optimum pitch angles. To the knowledge of the authors, there are no empirical corrections for a turbine operating at non-optimum conditions and, therefore, none of the results presented in this paper were corrected for blockage; this fact should be borne in mind when considering the power and thrust data.

The model turbine in the present work was supported by a single stanchion with a diameter, D_s, of 50 mm. The stanchion pierced the water surface above the turbine, as shown in Fig. 1. Its connection to the turbine housing may be seen in Fig. 2. In contrast, full-scale turbines would be supported in different ways, for example using piled jacket or gravity-based structures or monopile foundations [33].

As expected in the present tests, there was a localised disturbance of the water surface around the model stanchion in both the current-alone and wave-current cases, with a run-up on the upstream side of the support and a drawdown in its lee. This surface effect served to increase the loading on the stanchion above that expected if the surface remained undisturbed.

Chaplin and Teigen [34] studied the flow past a vertical surface-piercing circular cylinder with a large draught towed at steady speeds through water initially at rest. They concluded that the total resistance coefficient reached a maximum at a Froude number of about 1 (here defining the Froude number as $\overline{u}/\sqrt{gD_s}$), when that part of the loading that could be attributed to the presence of the free surface was equivalent to the submerged form drag on a length of cylinder of about $0.9D_s$.

In contrast to an increase in the loading on the supporting stanchion itself, Bahaj et al. [3] noted a small reduction in the thrust on a turbine with a shallow immersion (minimum depth to rotor tip of 19% of the rotor diameter, D) when compared to a turbine

with a deep immersion (minimum depth to rotor tip of 0.55*D*). There was a more significant reduction of 10–15% in the turbine's power coefficient. The authors attributed both reductions to the fact that the free surface acts like a reflecting plane, preventing the full expansion of the turbine wake, thus causing a reduction in the pressure difference across the device.

Whatever the effects of the water surface on the thrust and power measurements, the objective of the present work was to show how the blade pitch angle may be used to attenuate the wave-induced unsteady loads on a horizontal axis tidal stream turbine. This mechanism may be expected to apply regardless of any free-surface effects caused by the particular configuration of any supporting structure, though the precise degree of attenuation may vary.

4. Results

4.1. Wave–current characterization

The average wave surface characteristics were determined using the profiles measured across the width of the working section. Fig. 5a–c shows a collection of all measured wave cycles (~1200 waves) used to determine the average profiles of the three waveforms. The results showed that the waves produced were essentially regular, although the wave height could vary by ±5% and the wave period by ±0.5%. The resultant profiles, from the averages of all the wave cycles, were then compared with profiles from Stokes' second-order wave theory, as given by equation (3). Excellent agreement was found between experimental and theoretical results for waveforms 1 and 2, as shown in Fig. 5a and b. Waveform 3 had a profile that did not fully agree with Stokes' second-order theory. In Fig. 5c, waveform 3 is compared with a theoretical profile with the same wave height and period, determined using Equation (3). The differences between the theoretical and experimental profiles may occur because these relatively steep waves were artificially forced on the current and did not propagate a sufficient distance to reach a more natural state.

Direct measurements of the wavelengths were taken using two resistance probes placed downstream of the wavemaker separated by a distance equal to the wavelength calculated using equation (2). Data were recorded simultaneously by the resistance probes and it was observed that wave crests occurred essentially at the same time (within ±0.01 s), indicating that the calculated wavelengths agreed closely with the measured values.

The mean characteristics for the three experimental waveforms are given in Table 1, which shows that the tests were performed in intermediate water depths ($0.04 \leq d/L \leq 0.5$) and that waveform 3 represented moderately steep waves ($H/L \approx 0.06$). The values of the Ursell number, HL^2/d^3, were lower than unity so that good agreement with Stokes' theory was expected [25].

Direct measurements of the velocity components were taken through the water column for the different wave-current flows. All the measured velocity data had an average signal-to-noise ratio above 50 dB and, thus, only in a small number of cases was data filtering required. To filter the data, the phase-space threshold despiking method from Goring & Nikora [35], as modified by Wahl [36], was used. The maxima and minima of the measured and theoretical vertical and horizontal velocities are shown in Figs. 6 and 7. The experimental results include an error bar of ±1% which is the uncertainty in the measurements of mean velocity using an ADV. Both velocity components showed significant oscillations about the mean values, with waveform 3 (W&C 3) having the greatest fluctuations. From Fig. 6, it is clear that the wave-current flows were in a current-dominated regime (i.e. the wave-induced velocities were lower than the current velocity). The

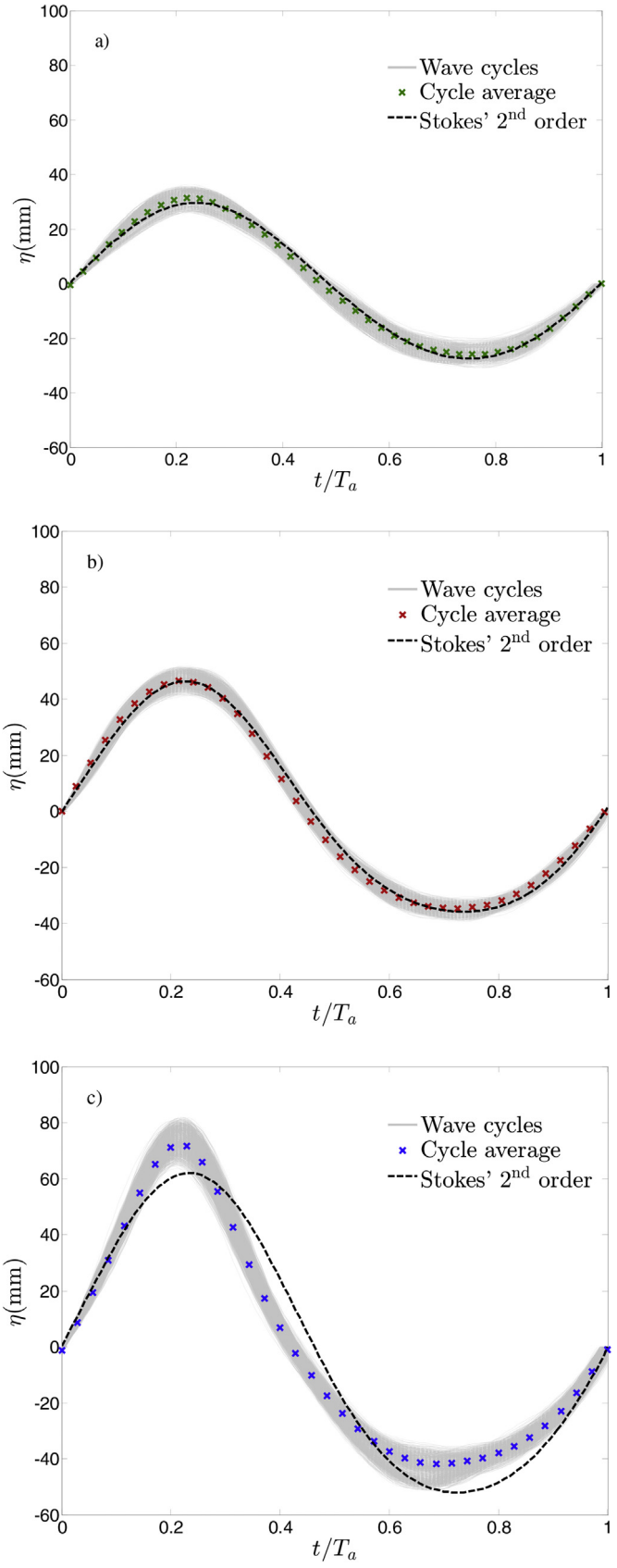

Fig. 5. Measured wave cycles with average and theory; a) waveform 1 b) waveform 2 c) waveform 3.

Table 1
Wave characteristics.

Waveform	H (m)	T_a (s)	L (m)	H/L	d/L	HL^2/d^3
1 (W&C 1)	0.058	0.81	2.25	0.026	0.34	0.67
2 (W&C 2)	0.082	0.75	2.00	0.041	0.38	0.75
3 (W&C 3)	0.113	0.69	1.75	0.065	0.43	0.79

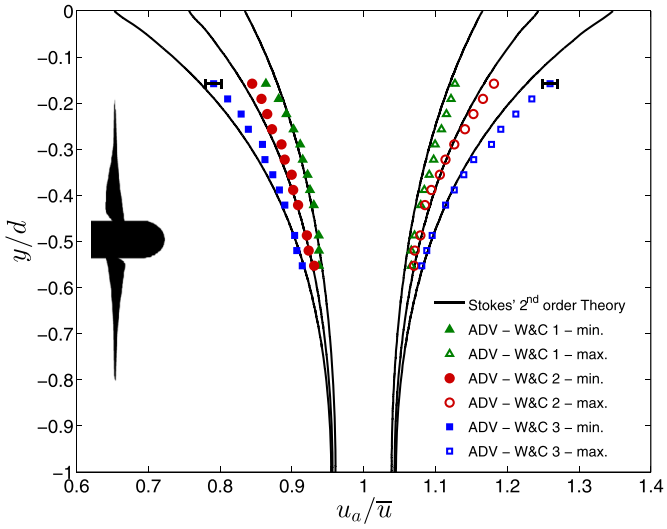

Fig. 6. Normalised results for measured and theoretical, maximum and minimum wave-induced horizontal velocities.

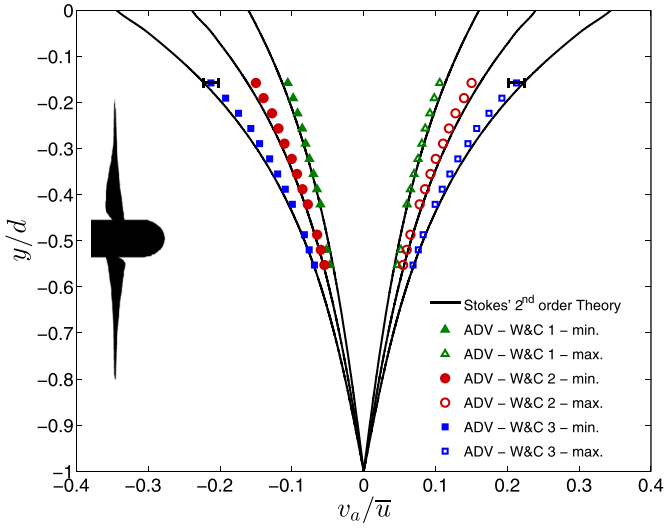

Fig. 7. Normalised results for measured and theoretical, maximum and minimum wave-induced vertical velocities.

measured velocities were compared with theory using equations (4) and (5), with the horizontal wave-induced velocities added linearly to the mean uniform current, as described by Umeyama [37]. It can be observed in Fig. 6 that there are small differences between the results near the surface, which are most evident for W&C 3. Nevertheless, overall good agreement was found between the theoretical and experimental results for both the horizontal and vertical velocities. The differences were always less than 2% of the mean streamwise velocity. Note that the calculated second-order corrections to the wave-induced kinematics were very small and therefore linear wave theory also provides good approximations to the measured velocities.

4.2. Power and thrust performance in torque-controlled mode

The rotor control system applies a constant resistive torque to the turbine; hence, as the water velocities fluctuate there will be corresponding fluctuations in the turbine's rotational speed, as shown in Fig. 8 for W&C 3. The corresponding fluctuations in the power and thrust coefficients are shown in Fig. 9a & b. It is these fluctuations in the thrust on the turbine that are the concern from the point of view of structural loading and fatigue.

Mean power coefficients, calculated using mean values for water velocity and power, as defined in equation (7), are plotted in Fig. 10 for both the uniform flow and the different wave-current conditions. The optimum blade angle for this HATT was determined to be 6° [28]; thus the highest mean power occurred at this angle. Overall there is a decrease in $\overline{C}_P$ as the blade pitch angle increases and an associated decrease in turbine rotational speed. For each angle, the mean power output for the different wave-current flows is very similar to that obtained in the uniform flow; certainly within the combined experimental uncertainties and the repeatability of a single experiment.

The standard deviations in the power coefficient (C'_P) for W&C 3, are plotted in Fig. 11 for the various blade angles studied. When the turbine was subject to waves and current, C'_P increased with power extraction and, as expected, it was much higher than under the current alone. C'_P was always highest under waveform 3 for all blade pitch angles, owing to the higher wave-induced velocities. The results for the power mean and standard deviation are consistent with previous studies [9–14,16–18]. Additionally, the results demonstrate a consistent decrease in C'_P as the pitch angle was increased when the turbine operated in the wave-current flows. The highest values of C'_P were observed at a pitch angle of 3°. Qualitatively similar results were observed for W&C 1 and 2.

Fig. 12 shows the probability density functions (PDFs) of the power data with the mean subtracted, for the different angles studied and at $\overline{C}_P = 0.54$. The PDFs are for data collected under W&C 3. The PDFs have a bimodal distribution with a small asymmetry, which occurs because the wave profiles considered were vertically asymmetric (i.e. they had longer troughs and shorter crests than sinusoidal profiles; see Fig. 5c). Fig. 12 shows a reduction in the data spread as the blade pitch angle increases from

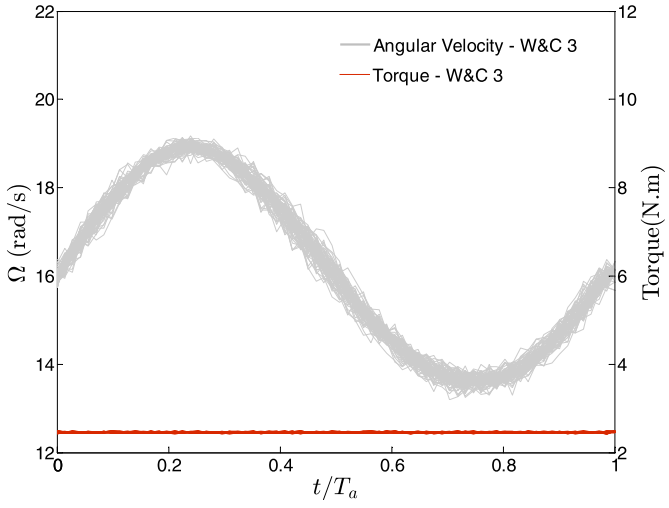

Fig. 8. Cycles of the turbine angular velocity and torque for W&C 3. The time is normalised by the apparent wave period.

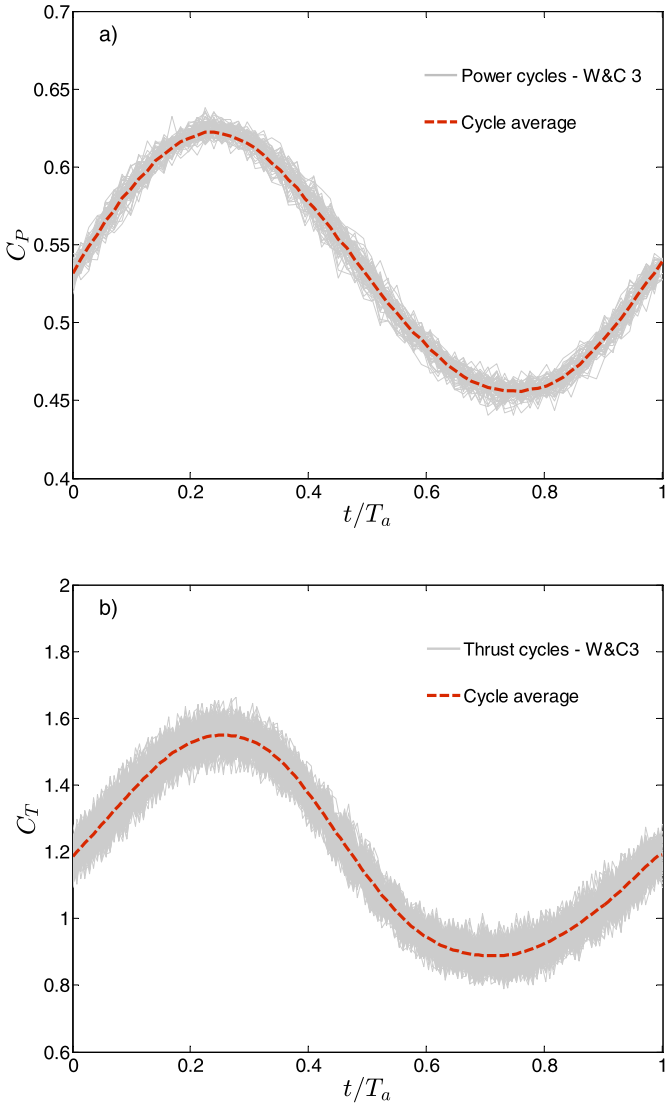

Fig. 9. Cycles for W&C 3 of the turbine coefficients with the cycle average; a) power; b) thrust.

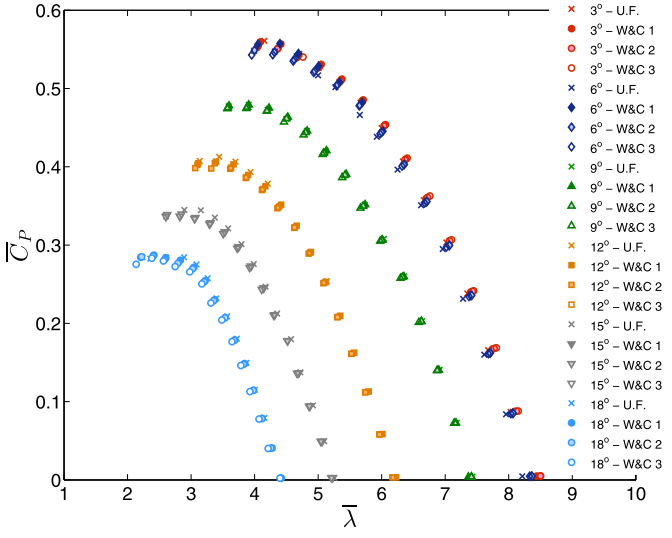

Fig. 10. Mean power coefficient for different blade pitch angles and flows.

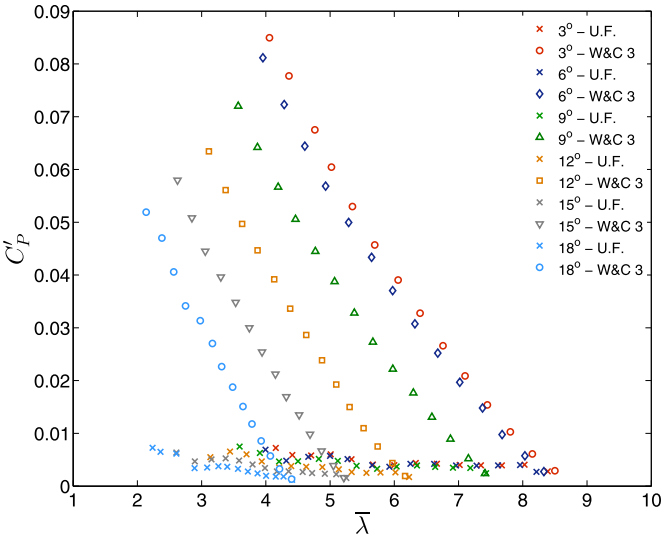

Fig. 11. Power coefficient standard deviation for different blade pitch angles under W&C 3.

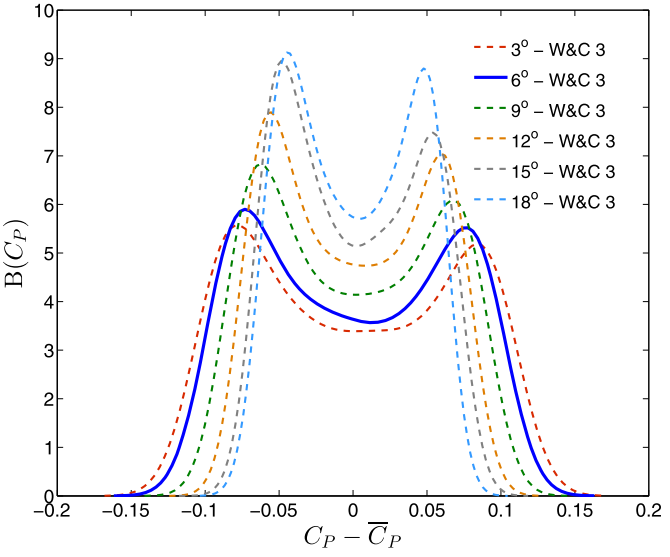

Fig. 12. Power coefficient probability density function (B) for W&C 3 at $\overline{C}_P = 0.54$ and $\overline{C}_T = 1.2$.

optimum and, thus, demonstrates an increase in the "steadiness" of the power output. Similar results were observed for the PDFs under the other wave-current flows, but with lower spreads in the data.

The spectra of the power data for the three different wave-current flows are plotted in Fig. 13 for the 6° optimum blade pitch angle at $\overline{C}_P = 0.54$. Unsurprisingly, the greatest oscillations in the power occurred under the highest wave-induced velocities (W&C 3) and in all three cases they were at the same frequency as the imposed waves. The spectra of the power data for non-optimum pitch angles showed similar trends but the magnitudes of the oscillations were lower for the higher-than-optimum pitch angles and also higher for the 3° angle.

Thrust data were collected for the same turbine settings and flow conditions as for the power measurements. Fig. 14 shows that, like the power coefficient, the mean thrust coefficient, $\overline{C}_T$, for a given blade pitch angle was not changed significantly by the presence of the waves. When the turbine blades were at the optimum pitch angle of 6°, $\overline{C}_T$ was fairly constant for the different

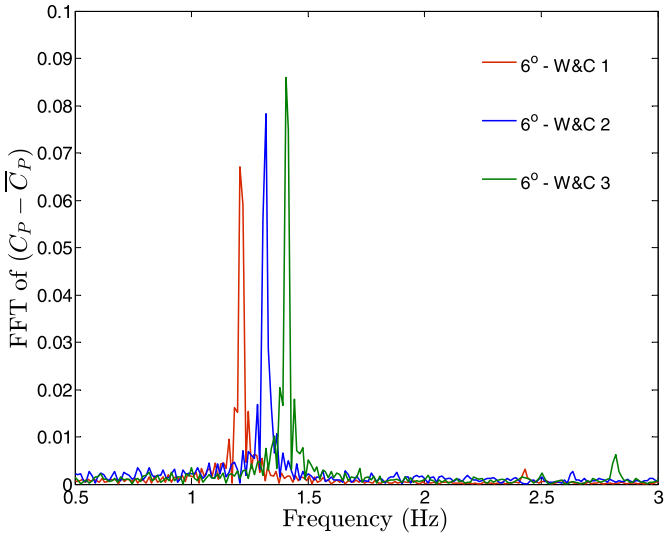

Fig. 13. Power spectral data at optimum blade pitch angle ($\overline{C}_P = 0.54$ and $\overline{C}_T = 1.2$.).

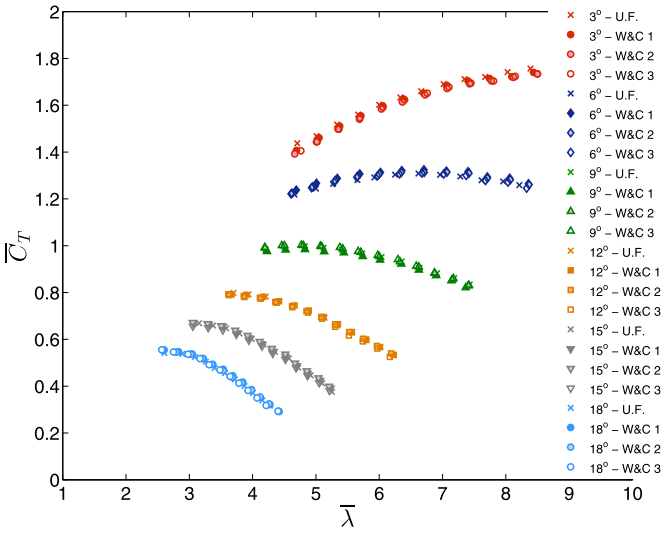

Fig. 14. Mean thrust coefficient for different blade pitch angles and flows.

turbine mean rotational speeds. However, for non-optimum pitch angles, $\overline{C}_T$ varies with the mean tip speed ratio,$\overline{\lambda}$, and hence with the power. For pitch angles greater than the optimum, $\overline{C}_T$ increases with increased power extraction while the opposite was observed for the angle lower than optimum. Regardless of the differences in the relationships between the thrust and rotational speed for non-optimum blade pitch angles, $\overline{C}_T$ always decreased as the blade pitch angle increased.

The standard deviations in the thrust coefficient (C'_T) for W&C 3, i.e. the magnitudes of the fluctuations and hence the source of the concern over fatigue, are plotted in Fig. 15. As expected, C'_T was much higher for waves and current than for a steady uniform current alone. For the different blade pitch angles, C'_T was always highest under waveform 3, showing that the highest wave-induced velocities produce the largest fluctuations in loading. The thrust standard deviations were qualitatively the same for the other wave-current cases studied. For all the wave-current flows, C'_T decreases slightly with decrease in $\overline{\lambda}$ for blade pitch angles lower than 12°, and increases slightly at higher angles. Overall, under the wave-current flows, C'_T decreases as the blade pitch angle increases.

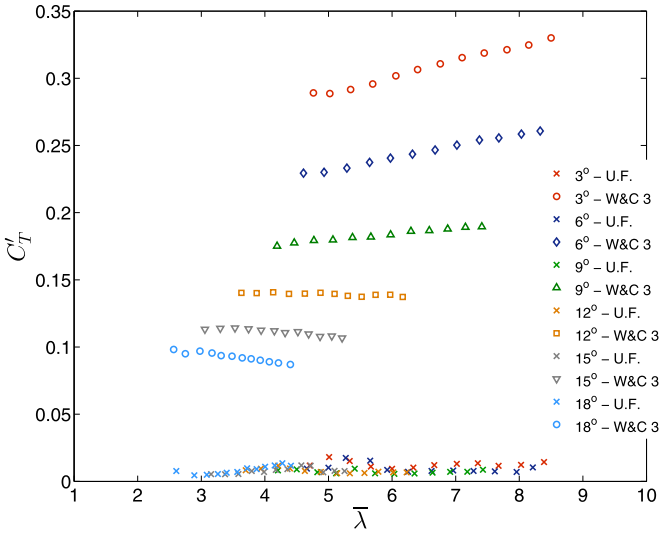

Fig. 15. Thrust coefficient standard deviation for different blade pitch angles under W&C 3.

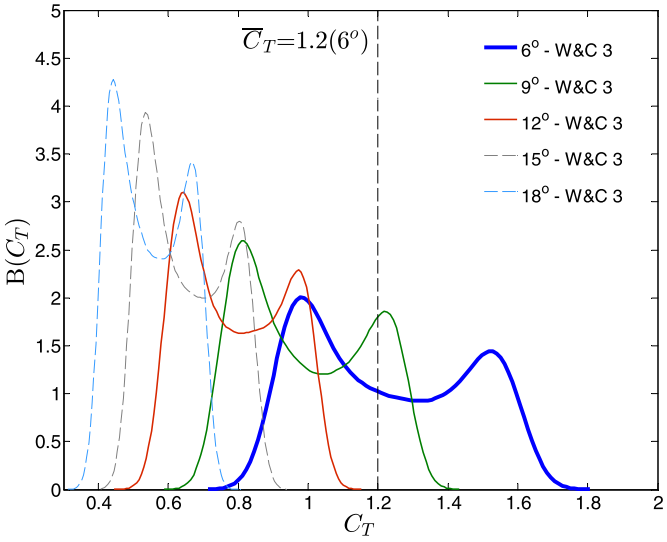

Fig. 16. Thrust coefficient probability density function (B) for blade pitch angles between 6° and 18° under W&C 3 ($\overline{C}_P = 0.54$ and $\overline{C}_T = 1.2$).

The means and standard deviations are consistent with previous studies [9–18], but with the additional observation that there is a significant reduction in the fluctuating load as the pitch angle is increased from optimum, indicating an attenuation of the mean and wave-induced cyclic loading on the turbine.

Fig. 16 shows the PDFs of the thrust data for blade angles between 6° and 18° under W&C 3 at $\overline{C}_P = 0.54$ and $\overline{C}_T = 1.2$. As for the power, the data show a bimodal pattern but there is a greater asymmetry, which most likely occurs because the thrust is being measured on the whole turbine structure, including its support stanchion which passes through the water surface. There is a consistent decrease in the data spread as the pitch angle increases and it can be seen that for angles higher than or equal to 12° the maximum thrust is always lower than the mean thrust at the optimum angle.

Analysis of the thrust spectral data, also at $\overline{C}_P = 0.54$ and $\overline{C}_T = 1.2$, is presented in Fig. 17 for the different wave-current conditions and the optimum blade pitch angle. As observed in

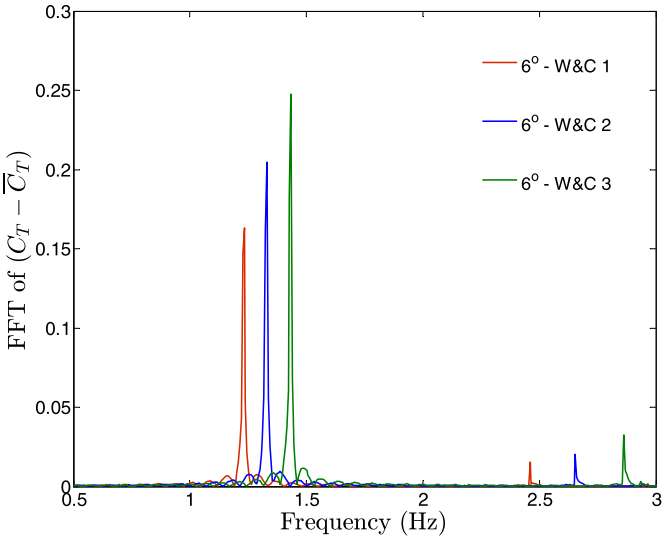

Fig. 17. Thrust spectral data for optimum blade pitch angle ($\overline{C}_P = 0.54$ and $\overline{C}_T = 1.2$).

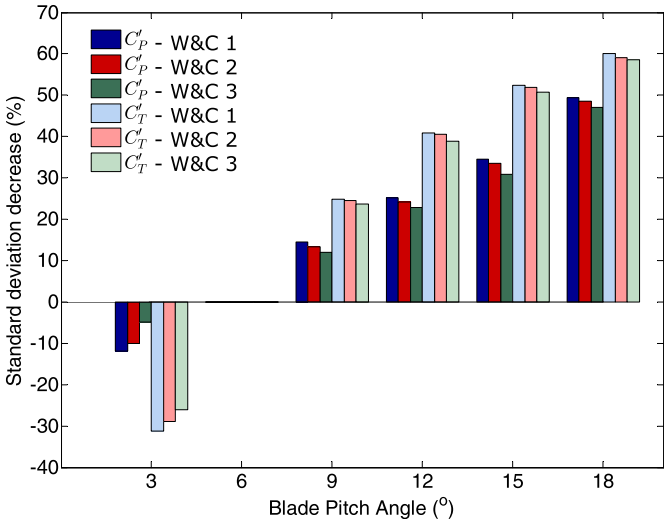

Fig. 19. Differences in the standard deviation of power and thrust coefficients from optimum blade pitch angle near peak-power output ($\overline{C}_P = 0.54$ and $\overline{C}_T = 1.2$).

the power results, the major oscillations occurred at the same frequency as the imposed waves and the greatest amplitudes were observed under the highest wave-induced velocities (W&C 3). As was the case for power, the spectra of the thrust data for non-optimum pitch angles showed similar trends, but with the amplitude of the oscillations decreasing as the blade pitch angle was increased.

5. Discussion

The purpose of the study was to assess whether the unsteady loading on a turbine in wave-current flows could be attenuated by adjusting the blade pitch angle, while avoiding too great a loss in the power output. The means and standard deviations of the power output and the loading on the turbine at non-optimum blade pitch angles were therefore compared with those for the optimum pitch angle at an operating point near peak-power output ($\overline{C}_P = 0.54$ and $\overline{C}_T = 1.2$, for optimum pitch). Fig. 18 shows the percentage change in the mean power output and thrust as the blade pitch angle is moved away from the optimum value of 6°. Fig. 19 shows the corresponding changes in the fluctuations in the power and thrust for the different blade angles.

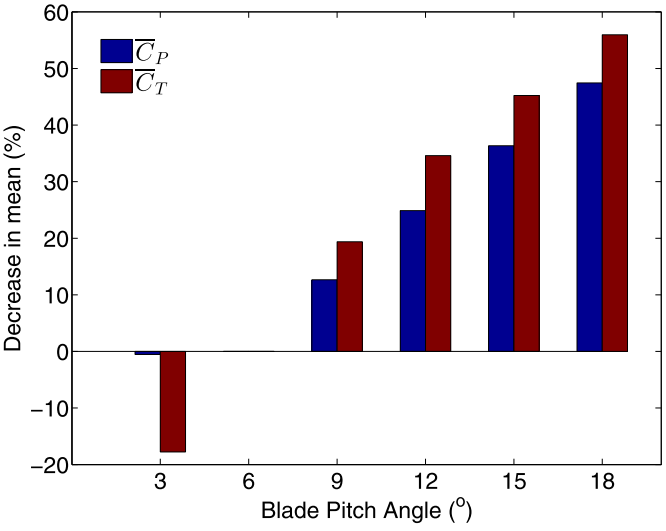

Fig. 18. Differences in the mean power and thrust coefficients from optimum blade pitch angle near peak-power output ($\overline{C}_P = 0.54$ and $\overline{C}_T = 1.2$).

In Fig. 18, when the blade pitch angle was decreased from optimum, $\overline{C}_P$ was essentially the same as for the optimum angle; however, there was a substantial increase in the mean thrust on the turbine. At the same time, Fig. 19 shows that when the turbine was operating under wave-current flows, C'_P and C'_T were much greater in all wave cases; the former indicates a reduction in the power "quality" (steadiness), while the latter indicates a greater threat from fatigue. However, as the blade pitch angle is increased away from the optimum, although there are substantial reductions in the mean power and thrust, Fig. 18 shows that the reductions in the mean thrust are always greater than in the mean power. For the wave-current flows, C'_P and C'_T also show significant reductions as the pitch angle is increased, as seen in Fig. 19. The reductions in the thrust standard deviations are always greater than in the corresponding power standard deviations, although the differences reduce as the pitch angle increases. Moreover, the reductions in C'_P and C'_T are always of a similar order for the same blade pitch angle regardless of wave-current condition.

The results indicate that the use of blade pitch angles higher than optimum can effectively reduce the mean load on the turbine while still permitting significant power extraction. Furthermore, increasing the blade angle can mitigate the fluctuations in the power output and the cyclic loading induced by surface waves, which in turn may help extend the lives of tidal stream turbines.

6. Conclusion and outlook

The purpose of the paper was to investigate if a technique used in the wind turbine industry could be adapted for use with tidal stream turbines; namely that by adjusting the blade pitch angle the unsteady loads caused by wave-current action could be attenuated without too much loss of power. The paper has presented an experimental investigation to evaluate the power and thrust performances of a model HATT using non-optimum blade pitch angles while subject to different wave-current flows. Three wave conditions were superimposed on a uniform steady current; their profiles and resultant induced kinematics were measured and two of the three were found to agree well with Stokes' second-order wave theory. The wave-current flows increased the fluctuations in both the power extracted and the loading on the turbine compared with

the current alone, although the effects on the mean values of power and thrust were negligible.

Increasing the blade pitch angle caused greater reductions in the mean thrust than in the mean power. There was also a substantial decrease of the magnitude of the power and thrust fluctuations. Therefore, changes in blade pitch angle can be used as a mechanism for reducing the loading on a HATT when operating with excessive wave-induced loads, while still enabling a significant amount of the available power in the unsteady tidal stream to be extracted.

Finally, in should be borne in mind that the results presented here were obtained using a *scale-model* under well-controlled laboratory conditions. We believe they represent an excellent "benchmark" data set which can be used by computational or theoretical modellers to validate their models prior to undertaking simulations of more realistic conditions both in terms of turbine support and channel geometry together with *in-situ* wave data. Earlier studies [28,29] have shown how the non-dimensional thrust and power data can be used, in conjunction with Reynolds number independent small-scale model data, to estimate power and thrust data for full-size turbines in current-alone conditions and we believe the data presented here could be used to predict forces on geometrically-similar full-scale turbines in identical wave-current conditions provided the Froude number is matched between the model and full-scale cases. Computational studies, such as those carried out recently by Tatum et al. [38], are necessary to fully test this hypothesis.

Acknowledgements

This study was performed under the research project "The Effects of Realistic Tidal Flows on the Performance and Structural Integrity of Tidal Stream Turbines", funded by the EPSRC (EP/J010200/1). The assistance provided by Siân C. Tedds, Richard Whalley, Gholamhossein Najafian, Emlyn Jones and Derek Neary is gratefully acknowledged.

References

[1] Carbon trust, tidal current resource and economics. U.K.: Black & Veatch; 2011. Tech. Rep.
[2] Bahaj AS, Meyers L. Power output performance characteristics of a horizontal axis marine current turbine. Renew Energy 2006;31:197–208.
[3] Bahaj AS, Molland AF, Chaplin JR, Batten WMJ. Power and thrust measurements of marine current turbines under various hydrodynamic flow conditions in a cavitation tunnel and a towing tank. Renew Energy 2006;32:407–26.
[4] Tedds SC, Owen I, Poole RJ. Near-wake characteristics of a model horizontal axis tidal stream turbine. Renew Energy 2014;63:222–35.
[5] Meyers LE, Bahaj AS. Experimental analysis of the flow field around horizontal axis tidal turbines by use of scale mesh disk rotor simulator. Ocean Eng 2010;37:218–27.
[6] Dean RG, Dalrymple RA. Water wave mechanics for engineers and scientists. 1984. New Jersey U.S.A.
[7] Hedges TS. Combinations of waves and currents: an introduction. ICE Part 1 1987;82:567–85.
[8] Svendsen IA, Jonsson IG. Hydrodynamics of coastal regions. Lyngby: Den Private ingeniørfond Technical University, Denmark; 1976.
[9] Barltrop N, Varyani KS, Grant A, Clelland D, Pham XP. Wave-current interactions in marine current turbines. IMechE Part M J Eng Marit Environ 2006:195–203.
[10] Barltrop N, Varyani KS, Grant A, Clelland D, Pham XP. Investigation into wave–current interactions in marine current turbines. IMechE Part A J Power Energy 2007:233–42.
[11] Galloway PW, Myers LE, Bahaj AS. Quantifying wave and yaw effects on a scale tidal stream turbine. Renew Energy 2014;63:297–307.
[12] Faudot C, Dahlhaug O. Prediction of wave loads on tidal turbine blades. Energy Procedia 2012;20:116–33.
[13] Luznik L, Flack KA, Lust EE, Taylor K. The effect of surface waves on the performance characteristics of a model tidal turbine. Renew Energy 2013;58:108–14.
[14] Lust EE, Luznik L, Flack KA, Walker JM, Van Benthem MC. The influence of surface gravity waves on marine current turbine performance. J Mar Energy 2013;3–4:27–40.
[15] Whelan JI, Graham JMR, Peiro J. Inertia effects on horizontal axis tidal-stream turbines. In: Proc. 8th European wave and tidal energy conference, Upsala, Sweden; 2009.
[16] Gaurier B, Davies P, Deuff A, Germain G. Flume tank characterization of marine current turbine blade behaviour under current and wave loading. Renew Energy 2013;59:1–12.
[17] Fernandez-Rodriguez E, Stallard TJ, Stansby PK. Experimental study of extreme thrust on a tidal stream rotor due to turbulent flow and with opposing waves. J Fluids Struct 2014;51:354–61.
[18] de Jesus Henriques TA, Tedds SC, Botsari A, Najafian G, Hedges TS, Sutcliffe CJ, et al. The effects of wave-current interactions on the performance of a model horizontal axis tidal turbine. J Mar Energy 2014;8:17–35.
[19] Bossanyi EA. Individual blade pitch control for load reduction. Wind Energy 2002;6:119–28.
[20] Bossanyi EA. Further load reductions with individual pitch control. Wind Energy 2005;8:481–5.
[21] Bossanyi EA, Fleming PA, Wright AD. Validation of individual pitch control by field tests on two- and three-bladed wind turbines. IEEE Trans Control Syst Technol 2013;21:1067–78.
[22] Marine Current Turbines Ltd. The SeaGen advantage. 2013. URL: http://www.marineturbines.com/sites/default/files/FINAL_MCT_Product_Brochure_8pp_Seagen_UPDATE_E_HIRes.pdf [online accessed: 30-March 2015].
[23] Scotrenewables–tidal power Ltd. Sr250 technology. 2014. URL: http://www.scotrenewables.com/technology-development/250kw-prototype/sr250-technology [online accessed: 30-March 2015].
[24] Andritz Hydro. Renewable energy from tidal currents. 2012. URL: http://www.andritz.com/hy-hammerfest.pdf [Online; accessed 30-March 2015].
[25] Hedges TS. Regions of validity of analytical wave theories. Proc ICE – Water Marit Energy 1995;112:111–4.
[26] A. Millward, The design and development of a recirculating water channel – a critical assessment, M.Phil thesis, Open University, Faculty of Technology, UK.
[27] Tedds SC, Poole RJ, Owen I, Najafian G, Mason-Jones A, Morris CE, et al. Experimental investigation of horizontal axis tidal stream turbines. In: Proc. 9th European wave and tidal energy conference, Southampton, UK; 2011.
[28] Mason-Jones A. Performance assessment of a horizontal axis tidal turbine in a high velocity shear environment. Ph.D thesis. Cardiff, UK: University of Cardiff; 2009.
[29] Mason-Jones A, O'Doherty DM, Morris CE, O'Doherty T, Byrne CB, Prickett PW, et al. Non-dimensional scaling of tidal stream turbines. Energy 2012;44:820–9.
[30] Mason-Jones A, O'Doherty DM, Morris CE, O'Doherty T. Influence of a velocity profile & support structure on tidal stream turbine performance. Renew Energy 2013;52:23–30.
[31] Voulgaris G, Trowbridge JH. Evaluation of the acoustic Doppler velocimeter (ADV) for turbulence measurements. J Atmos Ocean Technol 1998;15:272–89.
[32] Garrett C, Cummins P. The efficiency of a turbine in a tidal channel. J Fluid Mech 2007;588:243–51.
[33] Fraenkel PL. Power from marine currents. IMechE Part A J Power Energy 2002;216:1–14.
[34] Chaplin JR, Teigen P. Steady flow past a vertical surface-piercing circular cylinder. J Fluids Struct 2003;18:271–85.
[35] Goring DG, Nikora VI. Despiking acoustic Doppler velocimeter data. J Hydraul Eng 2002;128:117–26.
[36] Wahl TL. Discussion of 'Despiking acoustic Doppler velocimeter data'. J Hydraul Eng 2003;129:484–8.
[37] Umeyama M. Coupled PIV and PTV measurements of particle velocities and trajectories for surface waves following a steady current. J Waterw Port Coast Ocean Eng 2011;137:85–94.
[38] Tatum S, Frost C, O'Doherty D, Mason-Jones A, O'Doherty T. Modelling tidal stream turbines. In: Renewable energy in the service of mankind. Selected topics from the world renewable energy Congress WREC 2014, Vol. I. Springer; 2015. p. 351.